Structural and thermal control of seismic activity and megathrust rupture dynamics in subduction zones: Lessons from the Mw 9.0, 2011 Tohoku earthquake

Claudio Satriano, Viviana Dionicio, Hiroe Miyake, Naoki Uchida, Jean-Pierre Vilotte, Pascal Bernard

Structural and thermal control of seismic activity and megathrust rupture dynamics in subduction zones: Lessons from the Mw 9.0, 2011 Tohoku earthquake

Accepted manuscript

Earth and Planetary Science Letters, Volume 403, 2014, Pages 287-298
https://doi.org/10.1016/j.epsl.2014.06.037.

Authors:

Claudio Satriano[1], Viviana Dionicio[1], Hiroe Miyake[2], Naoki Uchida[3],

Jean-Pierre Vilotte[1], Pascal Bernard[1].

Affiliations:

[1] Institut de Physique du Globe de Paris, Sorbonne Paris Cité, Univ Paris Diderot, UMR 7154 CNRS, F-75005 Paris, France

[2] Earthquake Research Institute, University of Tokyo, Tokyo, Japan.

[3] Graduate School of Science, Tohoku University, Sendai, Japan.

Corresponding author:
Claudio Satriano
Institut de Physique du Globe de Paris,
1 Rue Jussieu
75238 Paris cedex 05, France
Tel: +33-1-83957726
Fax: +33-1-71937716/7717
Email: satriano@ipgp.fr

Abstract

The 2011 Tohoku megathrust earthquake ruptured a vast region of the northeast Japan Trench subduction zone in a way that had not been enough anticipated by earthquake and tsunami risk scenarios.

We analyzed the Tohoku rupture combining high-frequency back-projection analysis with low frequency kinematic inversion of the co-seismic slip. Results support the to-day well-accepted broadband characteristics of this earthquake. Most of the seismic moment is released during the first 100 s, with large co-seismic slip (up to 55 m) offshore Miyagi in a compact region on the landward side of the trench. Coherent high-frequency radiation areas and relatively low co-seismic slip are distinctive signature of the slab-mantle interface. The broadband characteristics of the Tohoku rupture are interpreted, integrating the seismic activity and structure information on the NE Japan forearc region, as signature of along-dip segmentation and segment interactions, that result from thermal structure, plate geometry, material composition and fracture heterogeneities along the plate boundary interface. Deep mantle corner flow and low dehydration rates along the cold subduction slab interface lead to an extended seismogenic slab-mantle interface, with strong bi-material contrast controlling larger propagation distance in the downdip preferred rupture direction. Off Miyagi, plate bending below the mantle wedge, ~142.3°E at ~25 km depth, is associated with the eastern limit of the deep M7-8-class thrust-earthquakes, and of the strongest coherent high-frequency generation areas. The region of the slab-crust interface between the mantle wedge limit, ~142.7°E at ~20 km depth, and a trenchward plate bending, ~143.2°E at ~15 km, acted as an effective barrier resisting for many centuries to stress-loading gradient induced by deep stable sliding and large earthquakes along the slab-mantle interface. The 2011 Tohoku earthquake, whose hypocenter is located on the east side of the mantle wedge limit, released the accumulated stress in this region and succeeded to overcome the plate bending, driving the upper plate boundary interface to slip co-seismically, regardless its frictional property, thanks to a combination of dynamic effects associated with bi-material rupture directivity and stress changes induced by reflection from the surface of waves released by the unstable slip. This conceptual framework provides elements for reappraisal of long-term seismic activity and occurrence of rare and extreme tsunamigenic megathrust in other subduction zones, like those of North-Central Lesser Antilles, Central and Northern Chile.

Keywords: 2011 Tohoku earthquake; Subduction; Earthquake rupture; Seismic cycle.

1. Introduction

The March 11, 2011 Mw 9.0 Tohoku earthquake is an extreme and rare event, the largest in Japan history, not only by its size but also by the challenges it presents to our understanding of megathrust rupture and of the seismic cycle in subduction zones. At the Japan Trench subduction zone, with a relatively long documented history of large earthquakes, no earthquake larger than magnitude 8.5 was previously known beside the M~8.5, 869 Jōgan earthquake (Minoura et al., 2001).

The reports of the Headquarters for Earthquake Research Promotion (Japan) included – based on historical seismicity and on the concept of segmentation of subduction (Ando 1975a; 1975b) – a maximum magnitude of 8.2, and issued, in early 2010, a specific probability (99% over 30 years) of an earthquake of magnitude around 7.8 off Miyagi Prefecture (Geller, 2011; Yomogida et al., 2011).

State-of-the-art seismic, geodetic, and mareographic measurements allowed for rapid convergence in the description and the extension of the rupture (e.g., Simons et al., 2011; Ide et al., 2011; Sato et al., 2011; Ozawa et al., 2011), which is characterized by an extremely compact region of large slip (between 30 and 60 meters) extending for ~100 km between the hypocenter and the trench, and 150 to 200 km along-strike (Koketsu et al., 2011; Yokota et al., 2011). Looking from closer distance and/or through high-frequency radiation, rupture complexity appears. By tracking travel-times on local strong motion records, several authors (Lee et al., 2011; Suzuki et al., 2011) inferred a rupture made of at least 3 or 4 sub-events, associated with asperities in the deeper part of the subduction zone (Asano and Iwata, 2012; Kurahashi and Irikura, 2013). Many studies (Honda et al., 2011; Ishii, 2011; Koper et al., 2011; Meng et al., 2011; Simons et al., 2011; Wang and Mori, 2011; Yao et al., 2011; 2012; 2013; Zhang et al., 2011; Maercklin et al., 2012; Roten et al., 2012; Yagi et al., 2012) have evidenced – using back projection techniques or related approaches – the deep origin of high-frequency radiation, reinforcing the idea of partitioning between deeper regions of high-frequency radiation and shallower large slip areas.

The mechanical and dynamic properties controlling the very high moment release within a small size region, together with the differentiation of the radiation in frequency are still a matter of debate, as well as a general framework for megathrust rupture complexity in relation to the variability of thermal structure and geometry of subduction zones (e.g. Lay et al., 2012; Yao et al., 2013).

In this paper we analyze the broadband rupture properties of the Tohoku earthquake, in light of background seismic activity, and of thermal and structural properties of the NE Japan forearc. A broadband image of the Tohoku rupture process is constructed from combining teleseismic back projection (0.2-0.5 Hz) and kinematic modeling of coseismic slip (0.002-0.3 Hz) (section 2). A reassessment of the space-time patterns of the pre-Tohoku seismicity – including seismic repeaters – is discussed together with a study of the radiation properties of some M > 6.5 events (section 3). We then interpret those results within a conceptual mechanical framework considering thermal structure, plate boundary geometry and compositional variations (section 4). We conclude discussing some of the implications of the proposed framework for the reappraisal of seismic and tsunami hazard in other subduction zones.

2. Rupture process of the Tohoku earthquake

2.1 Back projection analysis

We study high-frequency radiation from the rupture process through a back projection (BP) technique (Satriano et al., 2012), using teleseismic P-wave recordings at 217 stations of the Virtual European Broadband Seismograph Network (van Eck et al., 2004) and 706 broadband stations in North America, filtered in the 0.2-0.5 Hz and 0.5-4.0 Hz frequency bands (Figs. 1, S1).

Filtered signals are migrated back to the source using P-wave travel times from a 1-D global velocity model (Kennett et al., 1995). Station corrections, accounting for departures from 1D velocity model, are computed from multi-channel cross-correlation (VanDecar and Crosson, 1990) on the first-arrival P waveforms, preliminary aligned using theoretical AK135 travel-times from the JMA hypocenter (38.1035°N, 142.8610°W, 23.74 km depth, origin time: 2011-03-11T05:46:18.12 UTC). Traces are stacked using a 4-th root stacking technique (Xu et al., 2009), which enhances phase over amplitude coherency, improving resolution, but distorting the relative amplitude of energy peaks. The BP method has no resolution in depth: we will assume here that energy is radiated by rupture propagation on the coupled interface.

Results are shown in Fig. 1 as time-coded peaks of coherent energy. The four images are consistent in indicating two main stages of coherent high-frequency generation: (1) a relatively slow downdip propagation of high-frequency sources, at a speed of about 1.6 km/s, during the first 80 s; (2) a faster, along-strike expansion, at a speed of about 2.6 km/s. These two stages are reported in all the BP solutions available in literature. A third stage, around 160 s, is mainly seen in the “Europe 0.2-0.5 Hz” and “North-America 0.5-0.4 Hz” images, with coherent high-frequency sources moving updip at the southern end of the rupture, in agreement with other studies (e.g., Wang and Mori, 2011; Maercklin et al., 2012).

To confirm these observations, we analyzed the signal recorded by selected strong motion stations of KiK-net in Japan, similarly to Meng et al. (2011). Fig. 2b shows E-W acceleration envelopes aligned to the theoretical P-wave arrival time. Envelopes are computed from unfiltered acceleration signals, and then smoothed with a sliding 10 s window; for each trace, amplitude of the different arrivals is equalized over a sliding 30 s window. S-wave arrivals for selected BP peaks from the “Europe 0.2-0.5 Hz” image (Fig. 2a) are superimposed to the envelopes. Theoretical arrival times and observed phases are in good correspondence, even for the later sub-events at 123 s and 147 s, proving that they are not artifacts of the BP analysis. We recall that relative amplitude of BP peaks (circle size in Fig. 2a) is proportional to the 4-th root stack power and thus more related to the coherency of the stack, than to the actual energy of each sub-event.

2.2 Kinematic inversion driven by back projection

Inversion of fault slip from seismic observations usually requires selecting a-priori values for rupture kinematic parameters, such as extension and velocity. Resulting slip images depend on this choice (e.g., Lay et al., 2010a), and a robust way of fixing these parameters is essential. Back projection analysis can provide independent estimates of rupture extension and velocity, since it does not rely on them (Lay et

al., 2010b). The assumption is that coherent HF radiation is related to slip rate (or acceleration) and occurs (though not exclusively) near the tip of the propagating rupture (e.g., Spudich and Frazer, 1984; Vallée and Satriano, 2014).

Using the method by Kikuchi and Kanamori (1991), we explore the fault plane with a circular front propagating during the first 80 seconds at 1.6 km/s and, later, at 2.6 km/s, in accordance with BP results. The exploration front sets the earliest possible time at which a point on the fault can slip; actual rupture time and slip duration are controlled by the point source time duration, which is set to 48 s. Following the slab geometry imaged by Miura et al. (2005) for the subduction off-Miyagi, we define a two-plane fault model with dip angle of 10° above 27 km of depth and of 23° at larger depths. Strike angle is set to 203°, in accordance with the GCMT moment tensor solution (Nettles et al., 2011). The fault model is limited up dip by the trench axis; downdip extension, and south and north limits are set by the back projection peak locations (Fig. 3c). Search grid is made of cells of 20 x 20 km. See Supplementary Material for further details on source parameterization. Green's functions are computed for a layered structure (Lay et al., 2011), and seismic moment is converted to fault displacement using rigidity of 40 GPa for the shallower plane (weighted average of the upper velocity layers), and of 65 GPa for the deeper plane (value for the mantle wedge).

We model P-wave displacement recorded at teleseismic stations between 30 and 100 degrees from the epicenter (Fig. 3a) and filtered between 0.002 and 0.3 Hz. Waveform fit is excellent and displayed in the Supplementary Material, along with a test on the stability of the solution and a-posteriori comparisons between predicted and observed regional GPS displacement. From the analyses made in Supplementary Material, we infer that our kinematic slip model is robust and consistent for the main slip patch, but it possibly has too large slip for the southernmost patch. The latter is nonetheless a stable feature of the kinematic inversion, and it is required to correctly fit horizontal GPS direction and vertical displacement.

Estimated total moment is 5.0×10^{22} Nm, corresponding to Mw 9.1, which is a slight overestimate with respect to very long-period constraints, like the W-phase moment estimate of 4.26×10^{22} Nm (Duputel et al., 2011), corresponding to Mw 9.0. However, given the band-limited nature of body waves, we consider this result acceptable. The moment rate function (Fig. 3b) shows a weak initiation of the rupture (first 40 s); the main peak of moment release happens around 70 s and corresponds to the updip rupture propagation (Fig. 3c); moment release after 100 s is associated with along-strike rupture propagation. Fig. 3c shows the final slip distribution; more than 70% of the slip is concentrated between the epicenter and the trench axis, with maximum slip of about 55 m. This is consistent with the slip images obtained by modeling tsunami and geodetic data (Ito et al., 2011; Maeda et al., 2011; Fujii et al., 2011; Koketsu et al., 2011; Saito et al., 2011; Yokota et al., 2011; Romano et al., 2012; Sato et al., 2013) and by other kinematic slip inversions from teleseismic and/or regional strong motion and cGPS recordings (Ammon et al., 2011; Lay et al, 2011; Lee et al., 2011; Shao et al., 2011; Suzuki et al., 2011; Yoshida et al., 2011; Yagi and Fukahata, 2011; Yue and Lay, 2011).

In Fig. 3c, we compare the slip distribution with location of back projection peaks from European stations in the 0.2-0.5 Hz frequency band. High-frequency coherent radiation and large slip are

partitioned along dip, being located in the deeper part of the subduction and close to the trench, respectively. A similar repartition can be seen for all the BP images in Fig. 1.

3. The instrumental pre-Tohoku seismicity at Northeast Japan subduction zone

3.1 Historical earthquakes and Mw 7.2 Tohoku foreshock

Large interplate thrust-earthquakes (M > 6.4) are observed since 1931 along the subduction interface in the northeastern Japan forearc (Fig. 4a). Within the extent of the source resolution, a first set of ruptures (Fukushima-Oki sequence: M7.3, 1938; M7.0, 1938; Miyagi-Oki: M7.4, 1936; M7.1, 1937; M7.4 1978; M7.0, 2005) took place along the slab-mantle interface, some being interpreted as rupturing of persistent large-scale asperities that exist over multiple seismic cycles (e.g., Nagai et al., 2001; Yamanaka and Kikuchi, 2004). The other set occurred along the downdip part of the slab-crust interface (M7.0, 1981 Miyagi-Oki; M6.8, 2003 Fukushima; M7.5, 1938 Fukushima-Oki; and the Ibaraki events: M7.0, 1982; M6.4, 2008; M7.0, 2008).

We compare the radiation properties of the M9.0 mainshock and of the March 9 M7.3 largest foreshock with those of the 2003 M6.8 Fukushima and the 2005 M7.0 Miyagi-Oki earthquakes. The 2005 event is the latest of the Miyagi-Oki sequence at the slab-mantle interface. Its two asperities coincide or are in the vicinity of the two southern asperities of the 1978 M7.4 earthquake (e.g., Suzuki and Iwata, 2007; Wu et al., 2008), and are close to the 2011 high-frequency radiation generation areas identified by Kurahashi and Irikura (2013) and in this study. The 2003 Fukushima earthquake (Yamanaka and Kikuchi, 2004), along the downdip part of the slab-crust interface, is close to the epicenters of the Tohoku mainshock and of the largest foreshock.

For each earthquake, we analyze the regional velocity ground motions in the 0.2-0.5 Hz frequency band, at four K-NET stations (stations location in Fig. 2). Comparison of velocity amplitudes (Fig. 5) suggests about 5-to-10 times higher frequency generation for the 2011 Tohoku mainshock – for both the first and the second large wave packets – than during the 2005 event. On the other hand, comparable amplitude is observed between the 2003 M6.8 event and the 2011 M7.3 foreshock, suggesting HF depletion for the latter event. Both earthquakes generate relatively less high-frequency radiation than the 2005 M7.0 event, supporting the observation – from back projection – of relatively small HF generation along the slab-crust interface during the mainshock in hypocenter area. We also confirm a weak initial rupture start for the March 11, 2011 Tohoku mainshock – corresponding to an Mw 6.0 event (Chu et al., 2011), with fast slip and rupture velocity (Uchide, 2013) –, but not for the March 9, 2011 foreshock, nor for the 2003 and 2005 events (Fig. S8)

3.2 M3.5+ seismicity and Repeaters

We compile the M3.5+ background seismicity (Fig. 4b) from the catalogs of Tohoku University (January 1980 to September 1997) and JMA (October 1997 to March 7, 2011). The completeness magnitude is estimated to M3.5 in the landward area, and to M3.5–4.0 in the trenchward area (e.g., Hirose et al., 2002; Suzuki et al., 2011). We also reanalyze the catalog of repeating earthquake clusters from Uchida et al. (2009), to discriminate “persistent” clusters – spanning at least 20 years – (colored according to

their average recurrence time in Fig. 4b and S9b) from short-lived clusters, related to short-term transients (empty circles in Fig. S9b). Further details on the selection procedure are provided in Supplementary Material. Repeating earthquake clusters are thought to occur at small asperities on the fault zone that catch up with aseismic fault slip on the surrounding surface (Nadeau and McEvilly, 1999; Uchida and Matsuzawa, 2013).

Off Miyagi, between ~37.5°N and ~39.3°N, most of the persistent repeaters are located along the deep portion of the seismogenic slab-mantle boundary interface, and exhibit rather small recurrence times (up to 6-7 years), suggesting localized rapid creep loading around the M > 6.4 thrust asperities (Fig. 4a). In the same latitude range, most of the landward M3.5+ background seismicity is confined between the updip limit of stable repeaters and the mantle wedge limit, while most of the trenchward M3.5+ seismicity occurs between the mantle wedge limit and ~50 km from the trench. Close to the trench, depletion of background seismicity and absence of stable repeaters suggest a strengthening behaviour of the interplate.

South of 37.5°N, a trenchward extended region of dense persistent repeaters could be the signature of larger creeping areas along the slab-crust interface. At the south-end of the rupture zone, offshore Ibaraki, active M3.5+ seismicity in the shallower subduction might be related to the NE limit of the Philippine Sea plate, as it is further discussed in section 4.3.

4. A conceptual model for the HF and LF sources of the Tohoku 2011 earthquake

The dynamics and spatial extent of the 2011 Tohoku megathrust earthquake evidenced in this study are discussed here in the light of the pre-Tohoku seismicity, examined in the previous section, and of the state-of-knowledge provided by the many published studies on the thermal, petrophysical, and seismic structure of the northeast Japan subduction zone.

4.1 Structural and rheological along-dip segmentation offshore Miyagi

Offshore Miyagi – in the latitude range between ~37°N and 39°N – along-dip propagation of the Tohoku earthquake rupture is characterized by an updip region depleted in high-frequency and accommodating the largest co-seismic slip within a rather compact area, while the largest coherent HF sources remain confined downdip. In this latitude range, the subduction interface presents a number of prominent features, summarized in Fig. 6. From updip to downdip: the Trench, the backstop (B), a shallow plate bending (B1), the updip limit of the stagnant mantle wedge (W1), a deeper plate bending (B2), and the updip limit of the flowing mantle wedge (W2).

Large-scale seismic tomography, refraction and reflection studies (e.g., Ito et al., 2005; Huang et al., 2011; Zhao et al., 2011; Wang et al., 2012; Nakajima et al., 2013) reveal a transition between an updip high-Vp, low Vp/Vs, low-attenuation, stagnant mantle and a downdip low-Vp, high Vp/Vs, high-attenuation flowing mantle, with a boundary that meets the plate interface at 60-80 km of depth (W2), in agreement with numerical studies (e.g., Abers et al., 2006; Wada et al., 2008; Wada and Wang, 2009) aimed at explaining the surface heat flow in the NE Japan arc (Tanaka et al., 2004).

Receiver function images of the slab-mantle interface (Kawakatsu and Watada, 2007), between W1 and W2, show strong negative contrast between hydrous low-velocity oceanic crust material and

anhydrous high-velocity stagnant-mantle wedge material down to 60-80 km (W2) as a result of low slab dehydration and serpentinization rates (Reynard, 2013).

At smaller scales, seismic imaging studies (e.g., Yamamoto et al., 2011; Huang et al., 2011; Zhao et al., 2011; Wang et al., 2012) evidence spatial correlation between regions of high-Vp (low Vp/Vs) within the stagnant mantle wedge, and asperities of the large M7-8-class interplate deep earthquakes. Despite possible confusion between mixed mantle material properties and serpentinites (Reynard, 2013), regions of low-Vp (high Vp/Vs) within the stagnant mantle are interpreted in terms of higher degree and rates of serpentinization, possibly enhanced by fluid-saturated pore-and-fracture heterogeneities in the uppermost oceanic crust (Matsubara and Obara, 2011). This can lead to small-scale thin layers of serpentinite along the plate interface that can sustain creep deformation over long time-scales (Hilairet et al., 2007), and induce strong spatial variations of the interface coupling.

At the slab-mantle contact, a deep plate bending (B2) is evidenced by onshore-offshore wide-angle refraction and reflection experiments (Ito and al., 2005; Miura et al., 2005), around 142.3°E and ~25 km depth. In that vicinity (~141.5°-142.0°E) a trench-parallel short-scale low-Vp (low Vp/Vs) anomaly in the uppermost oceanic crust was identified (Matsubara and Obara, 2011), possibly linked to fluid-saturated pore-and-fracture heterogeneities (e.g., Takei, 2002).

The mantle-wedge limit (W1), at ~142.7°E and ~20 km depth, is associated with a smooth plate bending variation (Miura et al., 2005) and a low-Vp (low Vp/Vs) anomaly in the uppermost oceanic crust, interpreted as a fluid-saturated pore-and-fracture heterogeneity (Kennett et al., 2011; Matsubara and Obara, 2011). That limit is characterized by drastic change in material contrast along the interface — from stiff (slab-mantle) to weaker (slab-crust).

Updip from the mantle wedge limit (W1), a shallow plate bending (B1) is reported at ~143.2°E and ~15 km depth, where the dip of the plate boundary interface decreases from ~15° to ~5° (Ito et al., 2005). Beneath the accretion prism (B), the plate boundary interface may consist of thin and weak – low strength and shear stress – hydrated, clay-rich material layers (Chester et al., 2013).

4.2 Along-dip variations of seismogenic potential and friction

The reported M3.5+ seismic activity, including repeaters and large historical M7- and M8-class interplate earthquakes, provides further insight on the mechanical properties of the different along-dip segments of the subduction zone, and on their potential interactions (Fig. 6):

(1) The observed downdip limit of the seismicity at ~50-60 km (e.g., Igarashi et al., 2001) is consistent with the upper limit of the mantle corner flow (W2). Below, the creeping plate interface is associated with large-scale serpentinization, as evidenced from tomography and receiver function studies. This creeping section induces a gradient of loading along the plate boundary interface that decreases toward the trench.

(2) M3.5+ seismicity, fast persistent repeaters and large M7-8-class interplate earthquakes are confined along the slab-mantle interface (W2-B2). This seismicity is associated with high loading rates from the downdip creeping section below W2, and could be the signature of a patchwork of creeping

and locked frictional zones resulting from heterogeneities of composition within the stagnant mantle wedge, and dehydration and serpentinization rates at the upper boundary of the oceanic slab.

(3) Spatially heterogeneous, high-rate M3.5+ seismicity and lack of persistent repeaters along the slab-mantle interface between B2 and W1 suggest higher frictional strength and a more dominantly locked interface. The plate bending B2 is possibly associated with the upper limit of the rupture area of the M7-8-class interplate earthquakes occurring along the deeper segment W2-B2. This may result from: the geometrical barrier created by the bending at B2 with a larger strength-excess expected along the lower-dip segment beyond B2; the high bi-material contrast between the stiff mantle and the oceanic crust which favors rupture in the direction of the slip of the most compliant side, i.e., downdip (e.g., Ampuero and Ben-Zion, 2008). Downdip dynamic rupture propagation is indeed reported for most of the deep historical events (Nagai et al., 2001; Yamanaka and Kikuchi, 2003; 2004; EIC Seismological Note, 2007; Mochizuki et al., 2008). Repeated rupture arrest of large interplate earthquakes at the plate bending B2 may induce stress perturbation along the segment B2-W1 enhancing seismic activity and stress concentration at the mantle wedge limit.

(4) Seismic activity, including shallower M7-class interplate earthquakes but no persistent repeaters, along the slab-crust interface between W1 and B1, suggests a strongly coupled frictional weakening interface. Large interplate earthquakes remain confined within this segment as the result of: the geometrical barrier created by the ~10° plate bending B1 and the expected larger frictional strength-excess along the lower-dip segment beyond B1; the drastic change in material contrast along the plate interface at the mantle wedge limit W1.

(5) Depleted seismicity, slow short-lived repeaters, and evidence of transient creep events suggest a trenchward transition from frictional weakening to strengthening along the shallow slab-crust interface between B1 and B. The February-March 2011 swarm-like precursory sequence, driven by transient slow slip, before the March 9 largest foreshock, occurred near the bending point B1 (e.g., Ando and Imanishi, 2011; Kato et al., 2012; Suzuki et al., 2012; Marsan and Enescu, 2012). This suggests the existence of stress and/or frictional heterogeneities in the vicinity of the plate bending B2 and possibly a marginally stable slab-crust frictional interface.

(6) Almost no seismicity is observed from the backstop to the trench (segment B-T), supporting frictional strengthening interface with increasing competing rate-strengthening (viscous) friction effects along the contact between the sedimentary wedge and the subducting oceanic crust.

4.3 Mechanical scenario of the Tohoku earthquake

During the many-centuries megathrust seismic cycle, non-stationary stress heterogeneity evolution and concentration at the mantle wedge limit, offshore Miyagi, may have been enhanced by: (1) the M3.5+ seismic activity in the segment B2-W1 linked to the combined effect of creep and large M7-8-class interplate earthquakes downdip from B2; (2) the shallower M7-class interplate earthquakes, and M3.5+ seismic activity, along the slab-crust interface between W1 and B1 (Fig. 6). This favored the nucleation of the 2011 Tohoku earthquake at the eastern side of the mantle wedge limit W1, as also

proposed by Sato et al. (2013). Both downdip and updip dynamic rupture propagation was equally favored due to the inversion of the interface material contrast at W1.

Near and beyond the plate bending B2, strong high frequency generation areas and relatively small co-seismic slip during the rupture propagation, can be associated with the lower stress level and the reported structural and rheological heterogeneities along the slab-mantle interface, prone to perturb the dynamic rupture.

In contrast, eastward of W1, weak high-frequency radiation and very large co-seismic slip beyond the upper plate bending are main characteristics of the trenchward rupture propagation. The rupture overcomes the plate-bending barrier as a result of: (1) release of the large accumulated stresses in the segment W1-B1; (2) enhanced bi-material propagation directivity; (3) large dynamic stresses developed by the B1-B2 growing rupture. Beyond B1, transition from frictional weakening to strengthening may have hampered high-frequency generation. It is worth noting here that, after the Tohoku earthquake, the seismic activity changes drastically in the slab-crust segment with increasing off-plane normal-fault activity and almost no interplate aftershocks (Suzuki et al., 2012) suggesting a complete stress overshoot and bulk energy dissipation in the hanging wall.

However, further considerations are required to explain the very large co-seismic slip in the slab-crust segment and why it did not result into a proportionally large HF radiation.

From the kinematic point of view, this imposes a constant, scale-independent rise-time of 10 s or more, filtering out HFs, thus at odds with the standard kinematic w-square source models based on scale-dependent rise-time (e.g., Ruiz et al., 2011). From the dynamic point of view, this would suggest large effective critical slip distance *Dc* (5 m or more) along the frictional weakening interface, which may result from a combination of effects, such as wider dissipative plate boundary interface, or inelastic deformation in the hanging wall.

Towards the trench, beyond the plate bending B1, slip-time might increase as a result of increasing frictional rate-strengthening dissipation associated with mobilization of effective lubrication processes, reduction of effective normal stress toward the trench (Dmowska and Kostrov, 1973), dynamic stress changes associated with wave reflections from the surface (Kozdon and Dunham, 2003), and persistence of slow transient creep waves behind the rupture front (Clévédé et al., 2012). Other models (e.g., Shibazaki et al., 2011) invoke possible frictional transition, at sufficiently high slip velocity, from velocity strengthening to velocity weakening, or high-velocity thermal pressurization effects (Mitsui et al., 2012; Noda and Lapusta, 2013), which however may likely involve high-frequency generation.

Although our model bares some similarity with the generic framework proposed by Lay et al. (2012) and Yao et al. (2013) for depth-dependent frictional properties of megathrust faults, it stresses out the complex interplay between along-dip variations of plate geometry and segment interactions, heterogeneities of frictional properties, interactions between seismic and a-seismic deformation, along-dip strong bi-material contrast variations, and dynamic effects.

4.4 Southern and northern limits of the Tohoku rupture

The trench-parallel extent of the Tohoku co-seismic slip zone retrieved from this study (Fig. 3) is in good agreement with the results of Kato and Igarashi (2012), including significant downdip slip between ~36°N and ~37°N.

The northern limit of the rupture (~39°N) is associated with a low seismicity (Ye et al., 2012) and low-V anomaly region (Zhao et al., 2011) off-Sanriku. In this region, slow and ultra-slow thrust earthquakes were observed, related to fluids at the slab boundary (Kawasaki et al., 2001; Fujie et al., 2002). The northern M7.4 aftershock of March 11, 2011 (Fig. 3c) is located at the boundary between this low-V zone and a northern high-V zone with reported large historical earthquakes (see Fig. 4). These observations support our northern extension limit of the 2011 rupture.

To its far south, the rupture is bordered by updip coherent HF sources, in good correlation with the rupture asperities of the 1982 (M7.0) and 2008 (M7.0) Ibaraki interplate earthquakes, and a zone of high seismicity and persistent repeaters. The southern M7.7 aftershock of March 11 (Fig. 3c) is located at the northern edge of the off-Ibaraki low-V zone (Zhao et al., 2011), and at the eastern boundary of an oceanic low-V anomaly (Matsubara and Obara, 2011). That part of the plate boundary may have been arresting the rupture before the NE limit of the Philippine Sea plate, located ~50 km further south. This last zone defines a small southernmost segment weakly if not at all activated by the 2011 Tohoku earthquake.

5. Conclusions

We studied the 2011 Tohoku megathrust rupture combining back-projection imaging of coherent high-frequency radiation sources with low-frequency kinematic inversion of coseismic slip. We interpret the broadband characteristics of this rupture as the signature of along-dip segmentation and segment interactions, resulting from thermal and petrophysical structure, plate geometry and mechanical variations along the plate boundary interface.

The Tohoku earthquake nucleated at the east side of the stagnant mantle-wedge upper limit. Downdip, the rupture propagated along the stiff slab-mantle interface, with moderate coseismic slip and coherent high-frequency radiation. The slab-mantle interface features a shallower segment of high M3.5+ seismicity rate – between the mantle wedge limit and a deep plate bending –, and a deeper segment of M7-8 class earthquakes and persistent repeaters, with strong coupling heterogeneities resulting from variations of mantle composition and interface serpentinization. Updip, the rupture propagated along the slab-crust interface, with very large coseismic slip toward the trench and no detectable high-frequency sources. The slab-crust interface is characterized by a seismogenic segment – between the mantle wedge limit and a shallow plate bending –, with M7-class ruptures and moderate M3.5+ earthquakes, and by segments of decreasing seismic activity toward the trench. The updip rupture overcame the plate-bending barrier as a result of finite rupture size and bi-material effects. Unstable deep slip succeeded in driving the upper frictional strengthening portion of the plate boundary interface to slip co-seismically as a result of dynamic wave interaction effects and reduction of normal stress toward the trench. High-frequency radiation may have been hampered by long-rise

time and hanging wall dissipation. Slip may have been enhanced by transient creep waves behind the rupture front.

In cold and fast subduction zones, like NE Japan, deep stable sliding, inducing a gradient of tectonic loading along the plate boundary interface, may lower the probability of nucleation of shallow tsunamigenic events (M7.5-8.5). Tsunami hazard must however be reevaluated in light of the ability of unstable deep slip to drive the shallower plate interface to slip co-seismically.

The Tohoku earthquake provides elements for future reappraisal of long-term seismic activity and occurrence of rare tsunamigenic megathrust events in other subduction zones. A first example is North-Central Lesser Antilles (Laigle et al., 2013), where the subducting cold slab is associated with low rates of slab dehydration and mantle serpentinization, deep mantle corner flow, inducing an extended seismogenic slab-mantle interface and similar along-dip plate boundary segmentation. A second example is Central Chile (Comte et al., 1986; Beck et al., 1998) and Northern Chile (Peyrat et al., 2010; Fuenzalida et al., 2013) where recent sequences of M7-8-class interplate earthquakes suggest along-dip segment interactions. Other examples are the cold-slab subduction along the Alaska-Aleutian zone, where along-dip segment interactions bear some similarities with Tohoku (Yomogida et al., 2011; Wada and Wang, 2009), and The Sumatra-Andaman subduction zone, which features along-strike segments with strong variations of slab-age and dehydration rates (Moeremans et al., 2014) suggesting trench-parallel variations of the along-dip segmentation.

Acknowledgements

We used the JMA earthquake catalog and strong motion data of K-NET and KiK-net from NIED. North America seismic data were obtained from the IRIS Data Management System. VEBSN seismic data was obtained from the ORFEUS Data Center. We thank A. Hirn, B. Reynard, S. Singh, and T. Yamashita for scientific discussions during this work. The research work that generated some of these results was founding by the 7th research program of the European community FP7/2007-2013 under the SP3-PEOPLE-Marie Curie-ITN QUEST-Grant Agreement Number 238007. Part of data analysis has been carried out using ObsPy (Megies et al., 2011). Figures have been realized using GMT (Wessel et al., 2013) and Matplotlib (Hunter, 2007).

References

Abers, G.A., van Keken, P.E., Kneller, E.A., Ferris, A., Stachnik, J.C., 2006. The thermal structure of subduction zones constrained by seismic imaging: Implications for slab dehydration and wedge flow. Earth Planet. Sci. Lett. 241, 387–397. doi: 10.1016/j.epsl.2005.11.055.

Ammon, C.J., Lay, T., Kanamori, H., Cleveland, M. 2011. A rupture model of the 2011 off the Pacific coast of Tohoku Earthquake. Earth Planets Space, 63(7), 693. doi: 10.5047/eps.2011.05.015.

Ampuero, J.P., Ben-Zion, Y., 2008. Cracks, pulses and macroscopic asymmetry of dynamic rupture on a bimaterial interface with velocity-weakening friction. Geophys J Int 173, 674–692. doi: 10.1111/j.1365-246X.2008.03736.x.

Ando, M., 1975a. Possibility of a major earthquake in the tokai district, Japan and its pre-estimated seismotectonic effects. Tectonophysics. 25, 69-85. doi: 10.1016/0040-1951(75)90011-6.

Ando, M., 1975b. Source mechanisms and tectonic significance of historical earthquakes along the Nankai Trough, Japan. Tectonophysics 27, 119–140. doi:10.1016/0040-1951(75)90102-X.

Ando, R., Imanishi, K., 2011. Possibility of Mw9.0 mainshock triggered by diffusional propagation of after-slip from Mw7.3 foreshock. Earth Planets Space 63, 767–771. doi: 10.5047/eps.2011.05.016.

Asano, K., Iwata, T. 2012. Source model for strong ground motion generation in 0.1-10 Hz during the 2011 Tohoku earthquake. Earth Planets Space. doi: 10.5047/eps.2012.05.003.

Beck, S., Barrientos, S., Kausel, E., Reyes, M., 1998. Source characteristics of historic earthquakes along the central Chile subduction zone. Journal of South American Earth Sciences 11, 2, 115-129.

Chester, F.M., et al., 2013. Structure and Composition of the Plate-Boundary Slip Zone for the 2011 Tohoku-Oki Earthquake. Science 342, 1208–1211. doi: 10.1126/science.1243719.

Chu, R., Wei, S., Helmberger, D.V., Zhan, Z., Zhu, L., Kanamori, H., 2011. Initiation of the great Mw 9.0 Tohoku–Oki earthquake. Earth Planet. Sci. Lett. 308, 277–283. doi: 10.1016/j.epsl.2011.06.031.

Clévédé, E., Bukchin, B., Favreau, P., Mostinskiy, A., Aoudia, A., Panza, G.F., 2012. Long-period spectral features of the Sumatra-Andaman 2004 earthquake rupture process. Geophys J Int 191, 1215–1225. doi: 10.1111/j.1365-246X.2012.05482.x.

Comte, D., Eisenberg, A., Lorca, E., Pardo, M., Ponce, L., Saragoni, G.R., Singh, S.K., Suarez, G., 1986. The 1985 central Chile earthquake: A repeat of previous great earthquakes in the region? Science 233, 449. doi: 10.1126/science.233.4762.449.

Dmowska, R., Kostrov, B. V., 1973. A shearing crack in a half-space under plane strain conditions, Arch. Mech. 25, 3, 421–440.

Duputel, Z., Rivera, L., Kanamori, H., Hayes, G.P., Hirshorn, B., Weinstein, S., 2011. Real-time W phase inversion during the 2011 off the Pacific coast of Tohoku Earthquake. Earth Planets Space 63, 535–539, doi: 10.5047/eps.2011.05.032.

EIC Seismological Notes, 2007, http://www.eri.u-tokyo.ac.jp/sanchu/Seismo_Note/index-e.html (last accessed 2013-05-21).

Fuenzalida, A., Schurr, B., Lancieri, M., Sobiesiak, M., Madariaga, R. 2013. High-resolution relocation and mechanism of aftershocks of the 2007 Tocopilla (Chile) earthquake. Geophys J Int. doi: 10.1093/gji/ggt163.

Fujie, G., Kasahara, J., Hino, R., Sato, T., Shinohara, M., Suyehiro, K., 2002. A significant relation between seismic activities and reflection intensities in the Japan Trench region. Geophys Res Lett 29, 1100. doi: 10.1029/2001gl013764.

Fujii, Y., Satake, K., Sakai, S., Shinohara, M., Kanazawa, T. 2011. Tsunami source of the 2011 off the Pacific coast of Tohoku Earthquake. Earth Planets Space, 63(7), 815–820. doi: 10.5047/eps.2011.06.010.

Geller, R.J., 2011. Shake-up time for Japanese seismology. Nature 472, 407–409. doi:10.1038/nature10105.

Hilairet, N., Reynard, B., Wang, Y., Daniel, I., Merkel, S., 2007. High-pressure creep of serpentine, interseismic deformation, and initiation of subduction. Science 318, 1910–1913. doi: 10.1126/science.1148494.

Hirose, F., Nakamura, A., Hasegawa, A., 2002. b-value variation associated with the rupture of asperities-spatial and temporal distributions of b-value east off NE Japan. Zisin 55, 249–260 (in Japanese with English abstract).

Honda, R., Yukutake, Y., Ito, H., Harada, M., Aketagawa, T., Yoshida, A., Sakai, S., Nakagawa, S., Hirata, N., Obara, K. 2011. A complex rupture image of the 2011 off the Pacific coast of Tohoku Earthquake revealed by the MeSO-net. Earth Planets Space, 63(7), 583–588. doi: 10.5047/eps.2011.05.034.

Huang, Z., Zhao, D., Wang, L., 2011. Seismic heterogeneity and anisotropy of the Honshu arc from the Japan Trench to the Japan Sea. Geophys. J. Int. 184, 1428–1444. doi:10.1111/j.1365-246X.2011.04934.x.

Hunter, J. D., 2007. Matplotlib: A 2D graphics environment, Comput. Sci. Eng., 9(3), 90–95, doi:10.1109/MCSE.2007.55.

Ide, S., Baltay, A., Beroza, G.C. 2011. Shallow Dynamic Overshoot and Energetic Deep Rupture in the 2011 Mw 9.0 Tohoku-Oki Earthquake. Science, 332(6036), 1426–1429. doi: 10.1126/science.1207020.

Igarashi, T., Matsuzawa, T., Umino, N., Hasegawa, A., 2001. Spatial distribution of focal mechanisms for interplate and intraplate earthquakes associated with the subducting Pacific plate beneath the northeastern Japan arc: A triple-planed deep seismic zone. J. Geophys. Res. 106, 2177–2191. doi:10.1029/2000JB900386.

Iinuma, T., Ohzono, M., Ohta, Y., 2011. Coseismic slip distribution of the 2011 off the Pacific coast of Tohoku Earthquake (M 9.0) estimated based on GPS data—Was the asperity in Miyagi-oki ruptured? Earth Planets Space. doi:10.5047/eps.2011.06.013.

Ito, A., Fujie, G., Miura, S., Kodaira, S., Kaneda, Y., Hino, R., 2005. Bending of the subducting oceanic plate and its implication for rupture propagation of large interplate earthquakes off Miyagi, Japan, in the Japan Trench subduction zone. Geophys. Res. Lett 32. doi:10.1029/2004GL022307.

Ito, T., Ozawa, K., Watanabe, T., Sagiya, T. 2011. Slip distribution of the 2011 off the Pacific coast of Tohoku Earthquake inferred from geodetic data. Earth Planets Space, 63(7), 627–630. doi: 10.5047/eps.2011.06.023.

Ishii, M. 2011. High-frequency rupture properties of the Mw9.0 off the Pacific coast of Tohoku Earthquake. Earth Planets Space, 63(7), 609–614. doi: 10.5047/eps.2011.07.009.

Kanamori, H., Miyazawa, M., Mori, J., 2006. Investigation of the earthquake sequence off Miyagi prefecture with historical seismograms. Earth Planets Space 58, 1533–1541.

Kato, A., Igarashi, T. 2012. Regional extent of the large coseismic slip zone of the 2011 Mw 9.0 Tohoku-Oki earthquake delineated by on-fault aftershocks. Geophys Res Lett, 39(15), L15301. doi: 10.1029/2012GL052220.

Kato, A., Obara, K., Igarashi, T., Tsuruoka, H., Nakagawa, S., Hirata, N., 2012. Propagation of Slow Slip Leading Up to the 2011 Mw 9.0 Tohoku-Oki Earthquake. Science 335, 705–708. doi: 10.1126/science.1215141.

Kawasaki, I., Asai, Y., Tamura, Y., 2001. Space–time distribution of interplate moment release including slow earthquakes and the seismo-geodetic coupling in the Sanriku-oki region along the Japan trench. Tectonophysics 330, 267–283. doi: 10.1016/S0040-1951(00)00245-6.

Kawakatsu, H., Watada, S., 2007. Seismic evidence for deep-water transportation in the mantle. Science 316, 1468–1471. doi: 10.1126/science.1140855.

Kennett, B.L.N., Engdahl, E.R., Buland, R., 1995. Constraints on seismic velocities in the Earth from traveltimes. Geophys. J. Int. 122, 108–124. doi:10.1111/j.1365-246X.1995.tb03540.x.

Kennett, B.L.N., Gorbatov, A., Kiser, E. 2011. Structural controls on the Mw 9.0 2011 Offshore-Tohoku earthquake. Earth Planet. Sci. Lett., 310(3-4), 462–467. doi: 10.1016/j.epsl.2011.08.039.

Kikuchi, M., Kanamori, H., 1991. Inversion of complex body waves-III. Bull. Seismol. Soc. Am. 81, 2335–2350.

Koketsu, K., H. Miyake, H. Fujiwara, and T. Hashimoto, 2008. Progress towards a Japan integrated velocity structure model and long-period ground motion hazard map, Proceedings of the 14th World Conference on Earthquake Engineering, Paper No.S10-038.

Koketsu, K., Yokota, Y., Nishimura, N., Yagi, Y., Miyazaki, S., Satake, K., Fujii, Y., Miyake, H., Sakai, S., Yamanaka, Y., Okada, T. 2011. A unified source model for the 2011 Tohoku earthquake. Earth Planet. Sci. Lett., 310(3-4), 1–8. doi: 10.1016/j.epsl.2011.09.009.

Koper, K.D., Hutko, A.R., Lay, T. 2011. Along-dip variation of teleseismic short-period radiation from the 11 March 2011 Tohoku earthquake (Mw 9.0). Geophys Res Lett, 38(21). doi: 10.1029/2011GL049689.

Kozdon, J.E., Dunham, E.M., 2013. Rupture to the Trench: Dynamic Rupture Simulations of the 11 March 2011 Tohoku Earthquake. Bull. Seismol. Soc. Am. 103, 1275–1289. doi: 10.1785/0120120136.

Kurahashi, S., Irikura, K., 2013. Short-period source model of the 2011 Mw 9.0 Off the Pacific coast of Tohoku earthquake. Bull. Seismol. Soc. Am. 103, 1373-1393. doi:10.1785/0120120157.

Laigle, M., Bayrakci, G., Evain, M., Hirn, A., Sapin, M., Bécel, A., Charvis, P., Flueh, E., Diaz, J., Lebrun, J.F., Gesret, A., Raffaele, R., Galvé, A., Ruiz, M., Kopp, H., Weinzierl, W., Hello, Y., Lépine, J.C., Viodé, J.P., Sachpazi, M., Gallart, J., Kissling, E., Nicolich, R., 2013. Seismic structure and activity of the north-central Lesser Antilles subduction zone from an integrated approach: Similarities with the Tohoku forearc. Tectonophysics 603, 1–20. doi: 10.1016/j.tecto.2013.05.043.

Lay, T., Ammon, C.J., Hutko, A.R., 2010a. Effects of kinematic constraints on teleseismic finite-source rupture inversions: Great Peruvian earthquakes of 23 June 2001 and 15 August 2007. Bull. Seismol. Soc. Am. 100, 969–994. doi:10.1785/0120090274.

Lay, T., Ammon, C.J., Kanamori, H., Koper, K.D., Sufri, O., Hutko, A.R., 2010b. Teleseismic inversion for rupture process of the 27 February 2010 Chile (Mw 8.8) earthquake. Geophys. Res. Lett 37, L13301. doi:10.1029/2010GL043379.

Lay, T., Ammon, C.J., Kanamori, H., Xue, L., Kim, M.J. 2011. Possible large near-trench slip during the 2011 Mw 9.0 off the Pacific coast of Tohoku Earthquake. Earth Planets Space, 63, 687–692. doi: 10.5047/eps.2011.05.033.

Lay, T., Kanamori, H., Ammon, C.J., Koper, K.D., Hutko, A.R., Ye, L., Yue, H., Rushing, T.M. 2012. Depth-varying rupture properties of subduction zone megathrust faults. J. Geophys. Res., 117, B04311. doi: 10.1029/2011JB009133.

Lee, S.-J., Huang, B.-S., Ando, M., Chiu, H.-C., Wang, J.-H., 2011. Evidence of large scale repeating slip during the 2011 Tohoku-Oki earthquake. Geophys. Res. Lett 38. doi:10.1029/2011GL049580.

Maeda, T., Furumura, T., Sakai, S., Shinohara, M. 2011. Significant tsunami observed at ocean-bottom pressure gauges during the 2011 off the Pacific coast of Tohoku Earthquake. Earth Planets Space, 63, 803–808. doi: 10.5047/eps.2011.06.005.

Maercklin, N., Festa, G., Colombelli, S., Zollo, A. 2012. Twin ruptures grew to build up the giant 2011 Tohoku, Japan, earthquake. Sci. Rep., 2. doi: 10.1038/srep00709.

Marsan, D., Enescu, B., 2012. Modeling the foreshock sequence prior to the 2011, M W9.0 Tohoku, Japan, earthquake. J. Geophys. Res. 117, B06316. doi: 10.1029/2011JB009039.

Matsubara, M., Obara, K. 2011. The 2011 off the Pacific coast of Tohoku Earthquake related to a strong velocity gradient with the Pacific plate. Earth Planets Space, 63, 663–667. doi: 10.5047/eps.2011.05.018.

Megies, T., Beyreuther, M., Barsch, R., Krischer, L., Wassermann, J., 2011. ObsPy – What can it do for data centers and observatories? Ann Geophys-Italy 54, 47–58. doi: 10.4401/ag-4838.

Meng, L., Inbal, A., Ampuero, J.-P. 2011. A window into the complexity of the dynamic rupture of the 2011 Mw 9 Tohoku-Oki earthquake. Geophys Res Lett, 38. doi: 10.1029/2011GL048118.

Minoura, K., Imamura, F., Sugawara, D., Kono, Y., Iwashita, T., 2001. The 869 Jogan tsunami deposit and recurrence interval of large-scale tsunami on the Pacific coast of northeast Japan. Journal of Natural Disaster Science, 23, 83–88.

Mitsui, Y., Kato, N., Fukahata, Y., Hirahara, K., 2012. Earth and Planetary Science Letters. Earth Planet. Sci. Lett. 325-326, 21–26. doi: 10.1016/j.epsl.2012.01.026.

Miura, S., Takahashi, N., Nakanishi, A., Tsuru, T., Kodaira, S., Kaneda, Y., 2005. Structural characteristics off Miyagi forearc region, the Japan Trench seismogenic zone, deduced from a wide-angle reflection and refraction study. Tectonophysics 407, 165–188. doi:10.1016/j.tecto.2005.08.001.

Mochizuki, K., Yamada, T., Shinohara, M., Yamanaka, Y., Kanazawa, T. 2008. Weak Interplate Coupling by Seamounts and Repeating M 7 Earthquakes. Science, 321(5893), 1194–1197. doi: 10.1126/science.1160250.

Moeremans, R., Singh, S.C., Mukti, M., McArdle, J., Johansen, K., 2014. Earth and Planetary Science Letters. Earth Planet. Sci. Lett. 386, 75–85. doi: 10.1016/j.epsl.2013.11.003.

Murotani, S., 2003. Rupture processes of large Fukushima-oki Earthquakes in 1938, Master's thesis, The University of Tokyo.

Nadeau, R.M., McEvilly, T.V., 1999. Fault slip rates at depth from recurrence intervals of repeating microearthquakes. Science 285, 718-721. doi: 10.1126/science.285.5428.718.

Nagai, R., M. Kikuchi, Y. Yamanaka, 2001. Comparative study on the source processes of recurrent large earthquakes in Sanriku-oki region: the 1968 Tokachi-oki earthquake and the 1994 Sanriku-oki earthquake, Zisin, 54, 267-280 (in Japanese with English abstract).

Nakajima, J., Uchida, N., Hada, S., Hayami, E., Hasegawa, A., Yoshioka, S., Matsuzawa, T., Umino, N., 2013. Seismic attenuation beneath northeastern Japan: Constraints on mantle dynamics and arc magmatism. J. Geophys. Res. 118, 5838–5855. doi: 10.1002/2013JB010388.

Nettles, M., Ekström, G., Koss, H.C. 2011. Centroid-moment-tensor analysis of the 2011 off the Pacific coast of Tohoku Earthquake and its larger foreshocks and aftershocks. Earth Planets Space, 63, 519–523. doi: 10.5047/eps.2011.06.009.

NGY seismological note, No. 7., 2008, http://www.seis.nagoya-u.ac.jp/sanchu/Seismo_Note/2008/NGY7.html (last accessed 2013-07-31).

Noda, H., Lapusta, N. 2013. Stable creeping fault segments can become destructive as a result of dynamic weakening. Nature, 493, 518-521. doi: 10.1038/nature11703.

Ozawa, S., Nishimura, T., Suito, H., Kobayashi, T., Tobita, M., Imakiire, T. 2011. Coseismic and postseismic slip of the 2011 magnitude-9 Tohoku-Oki earthquake. Nature, 475(7356), 373–376. doi: 10.1038/nature10227.

Peyrat, S., Madariaga, R., Buforn, E., Campos, J., Asch, G., Vilotte, J.-P., 2010. Kinematic rupture process of the 2007 Tocopilla earthquake and its main aftershocks from teleseismic and strong-motion data. Geophys. J. Int. 182, 1411. doi:10.1111/j.1365-246X.2010.04685.x.

Reynard, B. 2013. Serpentine in active subduction zones. Lithos, 178, 171–185. doi: 10.1016/ j.lithos.2012.10.012.

Romano, F., Piatanesi, A., Lorito, S., D'Agostino, N., Hirata, K., Atzori, S., Yamazaki, Y., Cocco, M., 2012. Clues from joint inversion of tsunami and geodetic data of the 2011 Tohoku-oki earthquake. Sci. Rep. 2, 385. doi:10.1038/srep00385.

Roten, D., Miyake, H., Koketsu, K. 2012. A Rayleigh wave back-projection method applied to the 2011 Tohoku earthquake. Geophys Res Lett, 39. doi: 10.1029/2011GL050183.

Ruiz, J.A., Baumont, D., Bernard, P., Berge-Thierry, C., 2011. Modelling directivity of strong ground motion with a fractal, k−2, kinematic source model. Geophys. J. Int., 186, 226–244. doi:10.1111/j.1365-246X.2011.05000.x.

Saito, T., Ito, Y., Inazu, D., Hino, R. 2011. Tsunami source of the 2011 Tohoku-Oki earthquake, Japan: Inversion analysis based on dispersive tsunami simulations. Geophys Res Lett, 38, L00G19. doi: 10.1029/2011GL049089.

Sato, M., Ishikawa, T., Ujihara, N., Yoshida, S., Fujita, M., Mochizuki, M., Asada, A. 2011. Displacement Above the Hypocenter of the 2011 Tohoku-Oki Earthquake. Science, 332(6036), 1395. doi: 10.1126/science.1207401.

Sato, T., Hiratsuka, S., Mori, J., 2013. Precursory Seismic Activity Surrounding the High-Slip Patches of the 2011 Mw 9.0 Tohoku-Oki Earthquake. Bull. Seismol. Soc. Am. 103, 3104–3114. doi: 10.1785/0120130042.

Satriano, C., Kiraly, E., Bernard, P., Vilotte, J.-P. 2012. The 2012 Mw 8.6 Sumatra earthquake: Evidence of westward sequential seismic ruptures associated to the reactivation of a N-S ocean fabric. Geophys Res Lett, 39(15), L15302. doi: 10.1029/2012GL052387.

Shao, G., Li, X., Ji, C., Maeda, T. 2011. Focal mechanism and slip history of the 2011 Mw 9.1 off the Pacific coast of Tohoku Earthquake, constrained with teleseismic body and surface waves. Earth Planets Space, 63, 559. doi: 10.5047/eps.2011.06.028.

Shibazaki, B., Matsuzawa, T., Tsutsumi, A., Ujiie, K., Hasegawa, A., Ito, Y., 2011. 3D modeling of the cycle of a great Tohoku-oki earthquake, considering frictional behavior at low to high slip velocities. Geophys Res Lett 38, L21305. doi: 10.1029/2011GL049308.

Simons, M., Minson, S.E., Sladen, A., Ortega, F., Jiang, J., Owen, S.E., Meng, L., Ampuero, J.-P., Wei, S., Chu, R., Helmberger, D.V., Kanamori, H., Hetland, E., Moore, A.W., Webb, F.H. 2011. The 2011 Magnitude 9.0 Tohoku-Oki

Earthquake: Mosaicking the Megathrust from Seconds to Centuries. Science, 332(6036), 1421–1425. doi: 10.1126/science.1206731.

Spudich, P., Frazer, L. 1984. Use of ray theory to calculate high-frequency radiation from earthquake sources having spatially variable rupture velocity and stress drop. Bull. Seismol. Soc. Am., 74, 2061–2082.

Suzuki, W., Iwata, T., 2007. Source model of the 2005 Miyagi-Oki, Japan, earthquake estimated from broadband strong motions. Earth Planets Space 59, 1155-1171.

Suzuki, W., Aoi, S., Sekiguchi, H., Kunugi, T. 2011. Rupture process of the 2011 Tohoku-Oki mega-thrust earthquake (M9.0) inverted from strong-motion data. Geophys Res Lett, 38. doi: 10.1029/2011GL049136.

Suzuki, K., Hino, R., Ito, Y., Yamamoto, Y., Suzuki, S., Fujimoto, H., Shinohara, M., Abe, M., Kawaharada, Y., Hasegawa, Y., Kaneda, Y., 2012. Seismicity near the hypocenter of the 2011 off the Pacific coast of Tohoku earthquake deduced by using ocean bottom seismographic data. Earth Planets Space 64, 1125–1135. doi: 10.5047/eps.2012.04.010.

Tanaka, A., Yamano, M., Yano, Y., Sasada, M., 2004. Geothermal gradient and heat flow data in and around Japan(I): Appraisal of heat flow from geothermal gradient data. Earth Planets Space 56, 1191–1194.

Takei, Y., 2002. Effect of pore geometry on VP/ VS: From equilibrium geometry to crack. J. Geophys. Res. 107, B2, 2043. doi: 10.1029/2001JB000522.

Uchida, N., Nakajima, J., Hasegawa, A., Matsuzawa, T., 2009. What controls interplate coupling?: Evidence for abrupt change in coupling across a border between two overlying plates in the NE Japan subduction zone. Earth Planet. Sci. Lett. 283, 111–121. doi:10.1016/j.epsl.2009.04.003.

Uchida, N., Matsuzawa, T., 2013. Pre- and postseismic slow slip surrounding the 2011 Tohoku-oki earthquake rupture. Earth Planet. Sci. Lett. 374, 81–91. doi: 10.1016/j.epsl.2013.05.021.

Uchide, T., 2013. High-speed rupture in the first 20 s of the 2011 Tohoku earthquake, Japan. Geophys. Res. Lett. 40, 2993–2997. doi: 10.1002/grl.50634.

Ueno, H., Hatakeyama, S., Aketagawa, T., Funasaki, J., Hamada, N. 2002. Improvement of hypocenter determination procedures in the Japan Meteorological Agency. Quart. J. Seism. 65, 123–134. (in Japanese).

Umino, N., Kono, T., Okada, T., Nakajima, J., Matsuzawa, T., Uchida, N., Hisegawa, A., Tamura, Y., Aoki, G., 2006. Revisiting the three M~7 Miyagi-oki earthquakes in the 1930s: possible seismogenic slip on asperities that were re-ruptured during the 1978 M= 7.4 Miyagi-oki earthquake. Earth Planets Space 58, 1587–1592.

Vallée, M., Satriano, C., 2014. Ten year recurrence time between two major earthquakes affecting the same fault segment. Geophys Res Lett 41, 2312–2318, doi: 10.1002/2014GL059465.

van Eck, T., Trabant, C., Dost, B., Hanka, W., Giardini, D. 2004. Setting up a virtual broadband seismograph network across Europe. Eos Trans. AGU 85, 125. doi:10.1029/2004EO130001.

Vandecar, J.C., Crosson, R.S., 1990. Determination of teleseismic relative phase arrival times using multi-channel cross-correlation and least squares. Bull. Seismol. Soc. Am. 80, 150.

Wada, I., Wang, K., He, J., Hyndman, R.D., 2008. Weakening of the subduction interface and its effects on surface heat flow, slab dehydration, and mantle wedge serpentinization. J. Geophys. Res. 113, B04402. doi: 10.1029/2007JB005190.

Wada, I., Wang, K., 2009. Common depth of slab-mantle decoupling: Reconciling diversity and uniformity of subduction zones. Geochem. Geophys. Geosyst. 10. doi: 10.1029/2009GC002570.

Wang, D., Mori, J. 2011. Rupture process of the 2011 off the Pacific coast of Tohoku Earthquake(Mw 9. 0) as imaged with back-projection of teleseismic P-waves. Earth Planets Space, 63, 603–607. doi: 10.5047/eps.2011.05.029.

Wang, Z., Huang, W., Zhao, D., Pei, S., 2012. Mapping the Tohoku forearc: Implications for the mechanism of the 2011 East Japan earthquake (Mw 9.0). Tectonophysics 524-525, 147–154. doi:10.1016/j.tecto.2011.12.032.

Wessel, P., Smith, W., Scharroo, R., Luis, J., Wobbe, F., 2013. Generic mapping tools: Improved version released. Eos 94, 409–410. doi: 10.1002/2013EO450001

Wu, C., Koketsu, K., Miyake, H., 2008. Source processes of the 1978 and 2005 Miyagi-oki, Japan, earthquakes: Repeated rupture of asperities over successive large earthquakes. J. Geophys. Res. 113, B08316. doi:10.1029/2007JB005189

Xu, Y., Koper, K.D., Sufri, O., Zhu, L., Hutko, A.R., 2009. Rupture imaging of the Mw 7.9 12 May 2008 Wenchuan earthquake from back projection of teleseismic P waves. Geochem. Geophys. Geosyst. 10, Q04006. doi:10.1029/2008GC002335.

Yamamoto, Y., Hino, R., Shinohara, M., 2011. Mantle wedge structure in the Miyagi Prefecture forearc region, central northeastern Japan arc, and its relation to corner-flow pattern and interplate coupling. J. Geophys. Res. 116. doi:10.1029/2011JB008470.

Yamanaka, Y., Kikuchi, M. 2003. Source process of the recurrent Tokachi-oki earthquake on September 26, 2003, inferred from teleseismic body waves. Earth Planets Space, 55(12), 21–24.

Yamanaka, Y., Kikuchi, M., 2004. Asperity map along the subduction zone in northeastern Japan inferred from regional seismic data. J. Geophys. Res. 109, 07307. doi:10.1029/2003JB002683.

Yagi, Y., Fukahata, Y. 2011. Rupture process of the 2011 Tohoku-oki earthquake and absolute elastic strain release. Geophys Res Lett, 38(19). doi: 10.1029/2011GL048701.

Yagi, Y., Nakao, A., Kasahara, A. 2012. Smooth and rapid slip near the Japan Trench during the 2011 Tohoku-oki earthquake revealed by a hybrid back-projection method. Earth Planet. Sci. Lett., 355-356(C), 94–101. doi: 10.1016/j.epsl.2012.08.018.

Yao, H., Gerstoft, P., Shearer, P.M., Mecklenbräuker, C. 2011. Compressive sensing of the Tohoku-Oki Mw 9.0 earthquake: Frequency-dependent rupture modes. Geophys Res Lett, 38(20). doi: 10.1029/2011GL049223.

Yao, H., Shearer, P.M., Gerstoft, P. 2012. Subevent location and rupture imaging using iterative backprojection for the 2011 Tohoku Mw 9.0 earthquake. Geophys. J. Int., 190(2), 1152–1168. doi: 10.1111/j.1365-246X.2012.05541.x.

Yao, H., Shearer, P.M., Gerstoft, P., 2013. Compressive sensing of frequency-dependent seismic radiation from subduction zone megathrust ruptures. PNAS 110, 4512–4517. doi: 10.1073/pnas.1212790110.

Ye, L., Lay, T., Kanamori, H. 2012. The Sanriku-Oki low-seismicity region on the northern margin of the great 2011 Tohoku-Oki earthquake rupture. J. Geophys. Res., 117(B2), B02305. doi: 10.1029/2011JB008847.

Yokota, Y., Koketsu, K., Fujii, Y., Satake, K., Sakai, S., Shinohara, M., Kanazawa, T. 2011. Joint inversion of strong motion, teleseismic, geodetic, and tsunami datasets for the rupture process of the 2011 Tohoku earthquake. Geophys Res Lett, 38. doi: 10.1029/2011GL050098.

Yomogida, K., Yoshizawa, K., Koyama, J., Tsuzuki, M., 2011. Along-dip segmentation of the 2011 off the Pacific coast of Tohoku Earthquake and comparison with other megathrust earthquakes. Earth Planets Space 63, 697–701. doi: 10.5047/eps.2011.06.003.

Yoshida, Y., Ueno, H., Muto, D., Aoki, S. 2011. Source process of the 2011 off the Pacific coast of Tohoku Earthquake with the combination of teleseismic and strong motion data. Earth Planets Space, 63(7), 565–569. doi: 10.5047/eps.2011.05.011.

Yue, H., Lay, T. 2011. Inversion of high-rate (1 sps) GPS data for rupture process of the 11 March 2011 Tohoku earthquake (Mw 9.1). Geophys Res Lett, 38, L00G09. doi: 10.1029/2011GL048700.

Zhang, H., Ge, Z., Ding, L. 2011. Three sub-events composing the 2011 off the Pacific coast of Tohoku Earthquake (Mw 9.0) inferred from rupture imaging by back projecting teleseismic P waves. Earth Planets Space, 63(7), 595–598. doi: 10.5047/eps.2011.06.021.

Zhao, D., Huang, Z., Umino, N., Hasegawa, A., Kanamori, H., 2011. Structural heterogeneity in the megathrust zone and mechanism of the 2011 Tohoku-oki earthquake (Mw 9.0). Geophys. Res. Lett 38. doi:10.1029/2011GL048408.

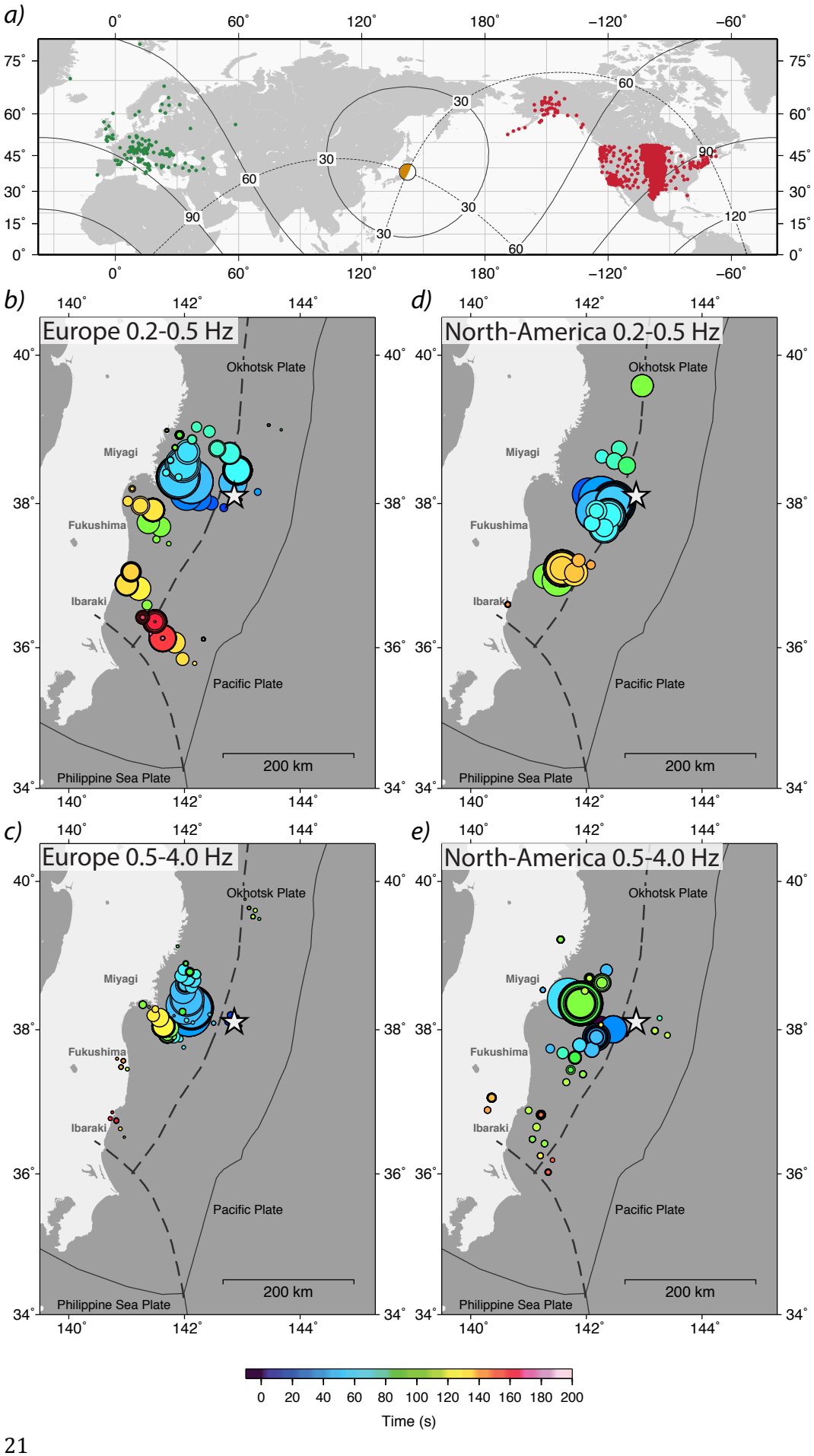
a)
b)
Europe 0.2-0.5 Hz
d)
North-America 0.2-0.5 Hz
c)
Europe 0.5-4.0 Hz
e)
North-America 0.5-4.0 Hz
Okhotsk Plate
Miyagi
Fukushima
Ibaraki
Pacific Plate
Philippine Sea Plate
200 km
0 20 40 60 80 100 120 140 160 180 200
Time (s)

Figure 1. Back projection (BP) imaging of the Tohoku earthquake. (a) Map of the stations from Europe and North America used for the analysis. (b–e) High-frequency coherent sources from the European stations (b, c), and the North-American stations (d, e), for two frequency bands (0.2-0.5 Hz and 0.5-4.0 Hz). Circles represent peaks of radiated energy coherently focused at the receiver array; their size is proportional to the power of the 4-th root BP stack used for the analysis. Peaks are colored by time in seconds from the earthquake origin. Solid lines are plate boundaries. Trench-parallel dashed line is the upper limit of the mantle wedge derived from the Japan Integrated Velocity Structure Model (Koketsu et al., 2008). The other dashed line is the NE limit of the Philippine Sea plate, as from Uchida et al. (2009). The star is the mainshock epicentral location from JMA.

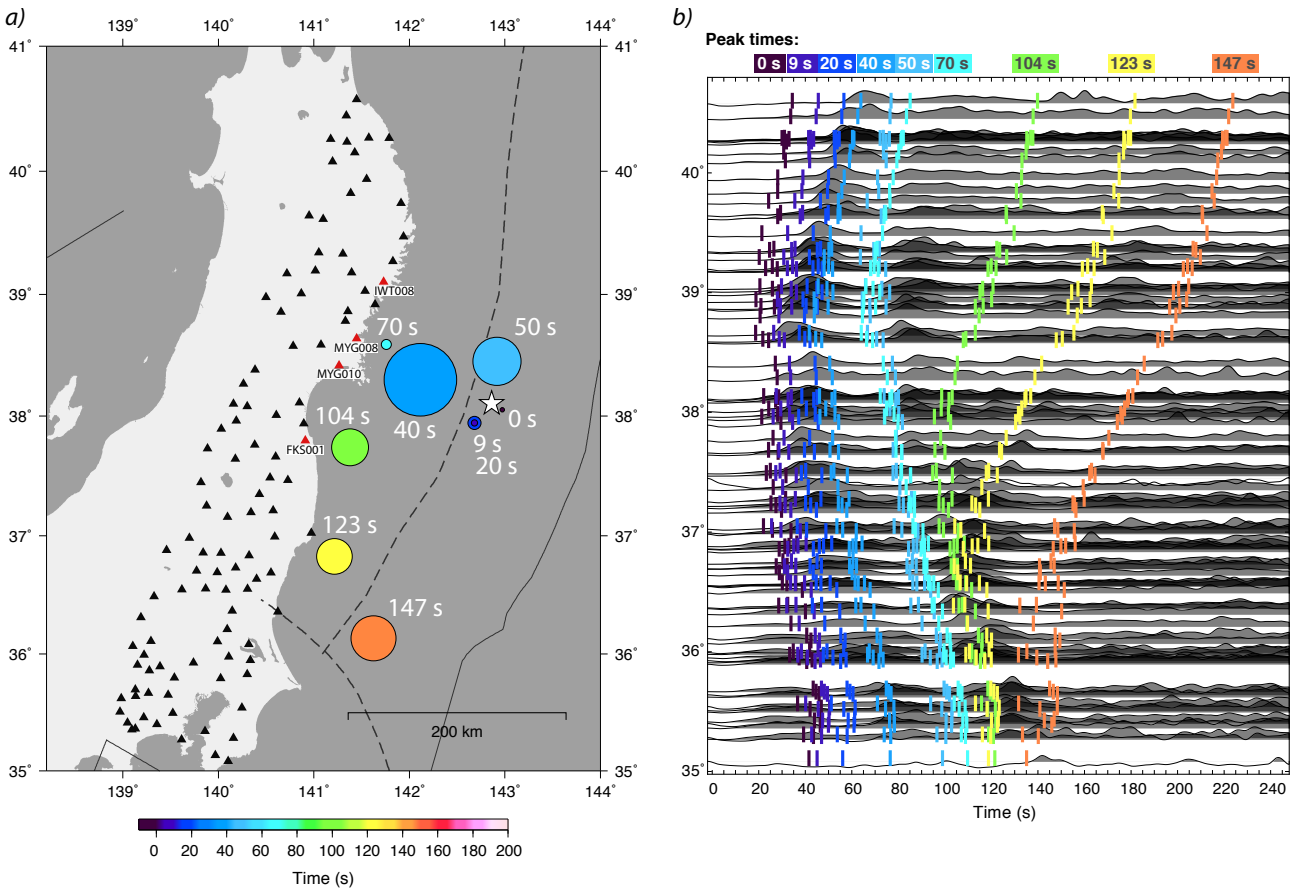

Figure 2. Comparison of the rupture process as seen from the European stations and by selected strong motion stations of KiK-net in Japan. (a) Circles: selected back projection peaks from European stations analysis in the band 0.2-0.5 Hz. As in Fig. 1, circle size is proportional to the power of the 4-th root stack used in the BP analysis. Triangles: selected strong-motion borehole stations from KiK-net. Red triangles, with labels, are K-NET stations used for the analysis of regional ground motion, shown in Figs. S7 and S8. Tectonic lines as in Fig. 1. (b) Smoothed E-W acceleration envelopes at the selected KiK-net stations, represented as a function of latitude and aligned to the theoretical P-wave arrival time from the JMA hypocenter. Original acceleration signals are unfiltered; envelopes are smoothed with a sliding 10 s window. For each trace, the amplitude of the different arrivals is equalized using automatic gain control (AGC) over a sliding 30 s window. Traces are then scaled to their maximum amplitude. Vertical bars indicate theoretical S-wave arrivals from the selected peaks and are colored according to the peak time. Theoretical P- and S-wave arrival times are calculated from the JMA 1D velocity model (Ueno et al., 2002).

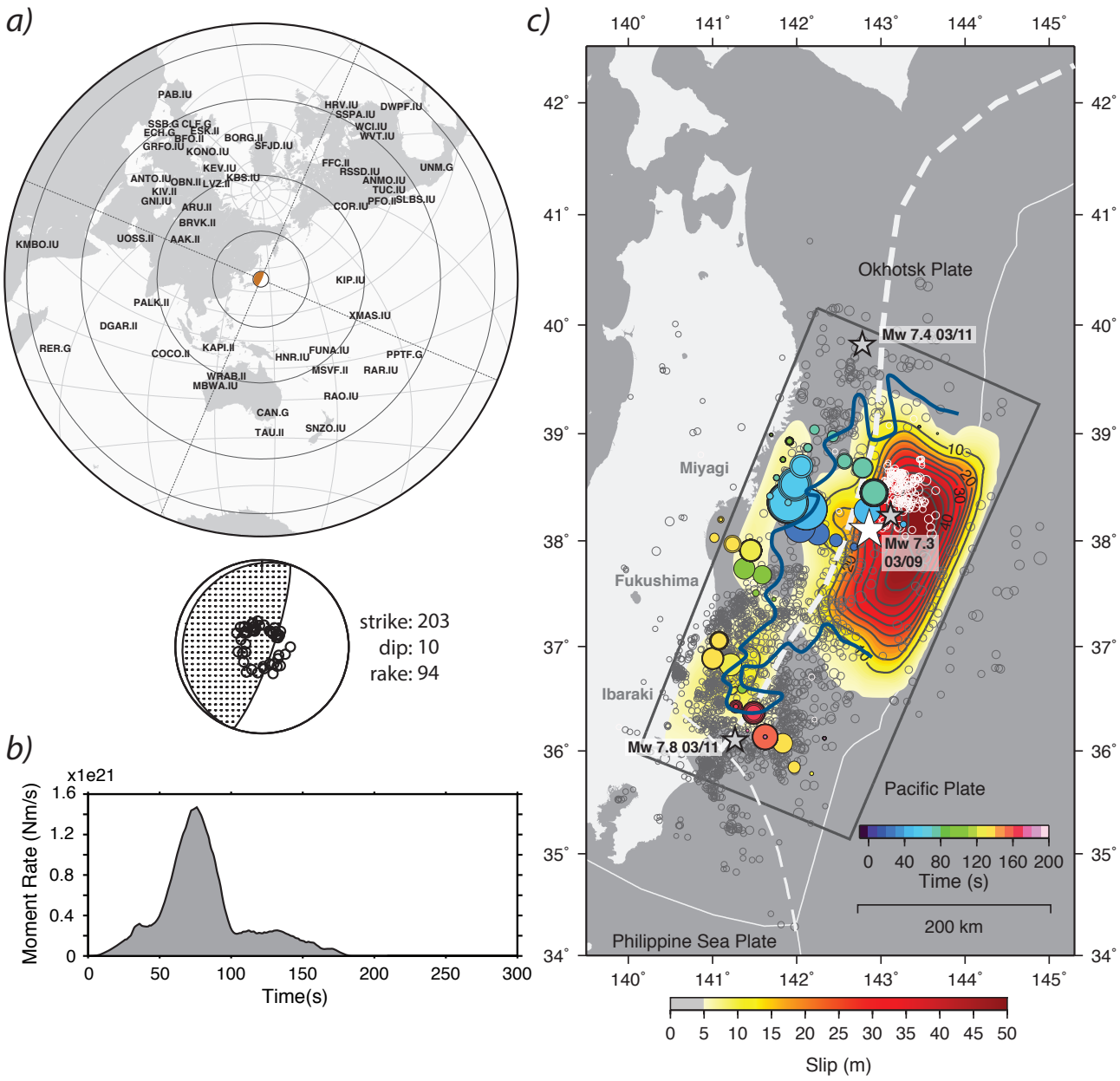

Figure 3. Kinematic slip inversion of the Tohoku earthquake. (a) Station distribution and focal sphere coverage. (b) Moment rate function, estimated total moment and corresponding moment magnitude. (c) Slip distribution and back projection peaks for the European stations in the frequency band 0.2 – 0.5 Hz. White and black open circles are, respectively, the locations of the foreshocks and aftershocks in the period from March 9, 2011 to March 21, 2011 from the JMA catalog. The largest foreshock of March 9 and the two large aftershocks of March 11 are indicated by stars. The blue line is the outer edge of the large-slip zone as determined by Kato and Igarashi (2012) from the analysis of the aftershock density distribution. Tectonic lines as in Fig. 1.

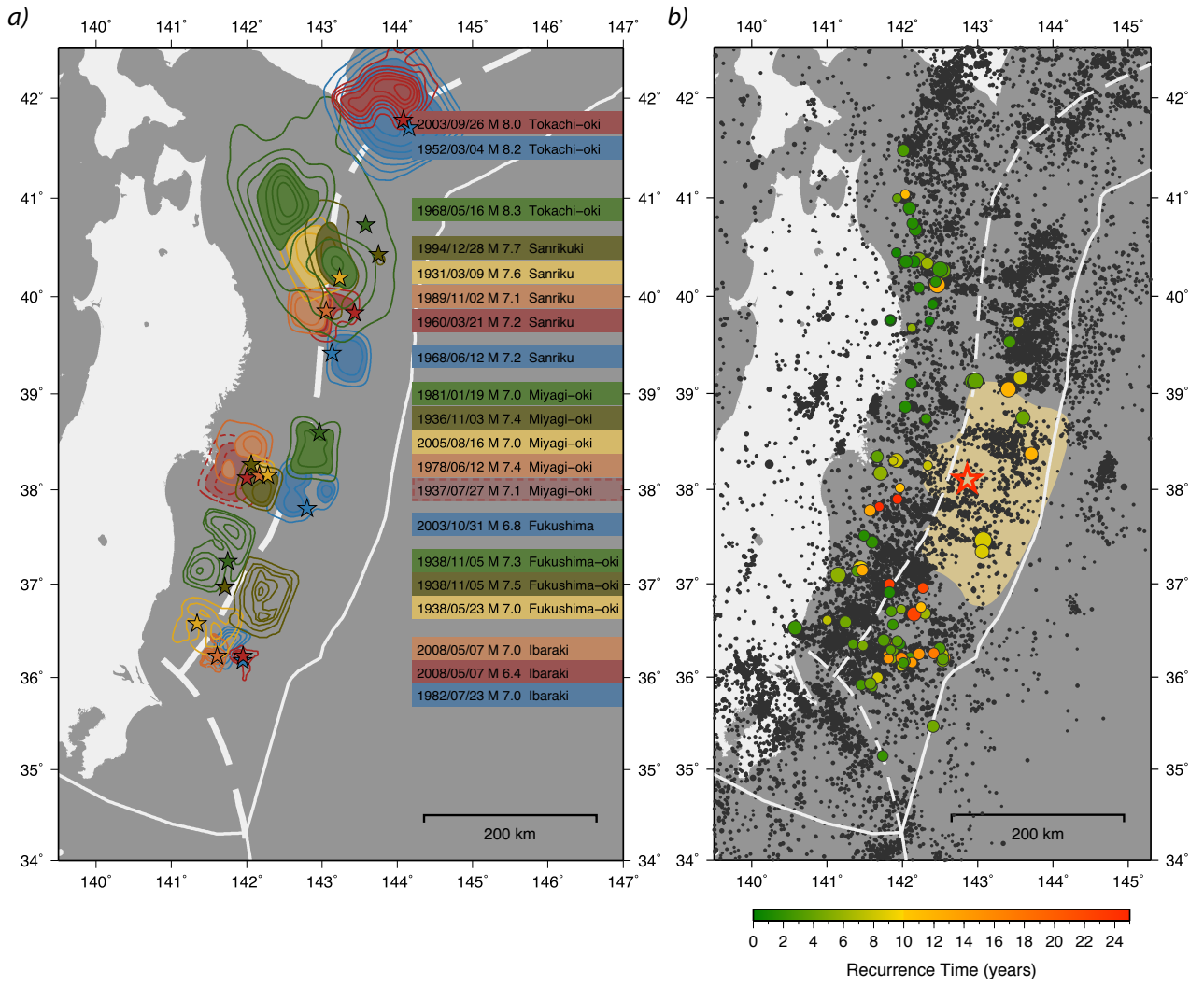

Figure 4. Instrumental pre-Tohoku seismicity at NE Japan. (a) Epicenters (stars) and rupture areas of 1931-2008 M6.4+ interplate earthquakes from the extent of their kinematic slip distribution (north of 37.5° from EIC Seismological Notes, 2007; Nagai et al., 2001; Yamanaka and Kikuchi, 2003; 2004; Fukushima-oki ruptures redrawn from Iinuma et al., 2011, after Murotani, 2003; the two Ibaraki 2008 ruptures from NGY Seismological Notes, 2008; Ibaraki 1982 from Mochizuki et al., 2008). M7.1, 1937 Miyagi-oki earthquake is shown with dashed lines, since it is still debated whether it is an intraplate or an interplate earthquake (Kanamori et al., 2006; Umino et al., 2006) (b) Epicentral distribution of M3.5+ earthquakes from the Tohoku University and JMA catalogs (black dots) and cluster locations of "persistent" repeating earthquakes (colored circles, see the text for the definition). Each circle represents the centroid location of a cluster; the circle size is proportional to the average magnitude; average recurrence time within each cluster is color-coded. Yellow region: largest slip area of the 2011 Tohoku earthquake (this study, see Fig. 3). Red star: epicenter of the 2011 Tohoku earthquake. Tectonic lines as in Fig. 1.

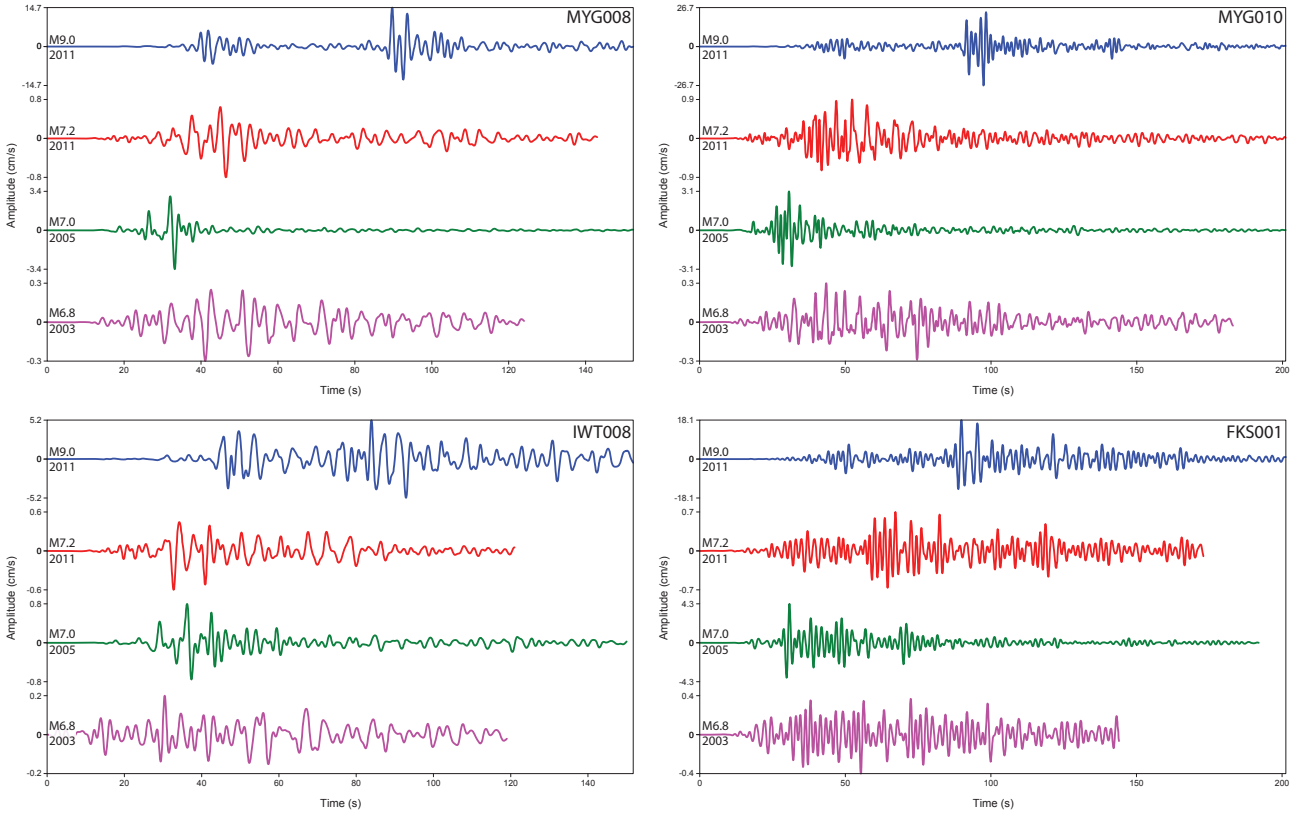

Figure 5. Velocity waveforms at K-NET stations MYG008, MYG010, IWT008 and FKS001 (see Fig. 3 for station location), obtained from time-integration of recorded acceleration. Shown are traces corresponding to the 2011 Mw 9.0 mainshock (blue), the 2011 Mw 7.2 foreshock (red), the 2005 Mw 7.0 Miyagi-oki earthquake (green), and the 2003 Mw 6.8 Fukushima earthquake (purple). Traces are filtered between 0.2 and 0.5 Hz. Note that vertical scale (in cm/s) is different from trace to trace.

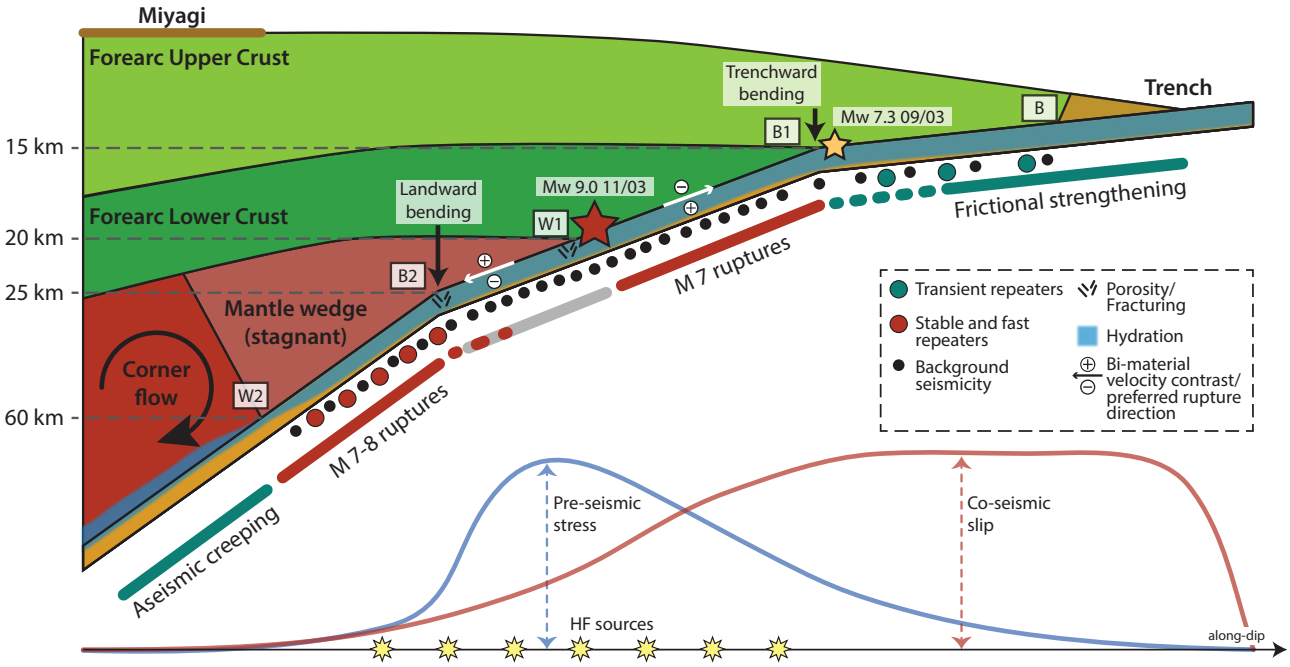

Figure 6. Schematic representation of segmentation and seismicity properties along the subduction offshore Miyagi. From updip to downdip: the Trench, the backstop (B), shallow plate bending (B1), the updip limit of the stagnant mantle wedge (W1), deep plate bending (B2), updip limit of the flowing mantle wedge (W2). The two curves on the bottom are schematic illustration of the pre-Tohoku stress profile (blue) and of the Tohoku coseismic slip profile (red). The zone of coseismic HF radiating sources is represented by yellow stars.